Journal of Power Sources 192 (2009) 684–688

Contents lists available at ScienceDirect

Journal of Power Sources

journal homepage: www.elsevier.com/locate/jpowsour

Short communication

X-ray diffraction study on Li_xCoO_2 below ambient temperature

K. Mukai[a,*], H. Nozaki[a], Y. Ikedo[a], J. Sugiyama[a], K. Ariyoshi[b], T. Ohzuku[b]

[a] Toyota Central Research and Development Laboratories, Inc., Yokomichi 41-1, Nagakute, Aichi 480-1192, Japan
[b] Department of Applied Chemistry, Osaka City University, Sugimoto 3-3-138, Sumiyoshi, Osaka 558-8585, Japan

ARTICLE INFO

Article history:
Received 26 August 2008
Received in revised form 2 March 2009
Accepted 3 March 2009
Available online 14 March 2009

Keywords:
Lithium-ion battery
Lithium cobalt oxide
X-ray diffraction
Synchrotron radiation

ABSTRACT

In order to elucidate the structural change of Li_xCoO_2 with temperature (T), powder X-ray diffraction measurements have been carried out using a synchrotron radiation source in the T range between 300 and 90 K for the samples with $x = 1.02$, 0.60, 0.56, and 0.53. The samples with $x < 1.02$ were prepared by an electrochemical reaction in a non-aqueous lithium cell. The $x = 1.02$ and 0.60 samples are in a rhombohedral phase ($R\bar{3}m$) in the whole T range measured. On the other hand, the $x = 0.56$ and 0.53 samples exhibit a structural transition around 140 K, although the both samples are in a monoclinic phase ($C2/m$) down to 90 K. That is, the angle between a_M- and c_M-axis (β_M) increases monotonically down to 150 K, then increases more rapidly with further lowering T. The values of $\Delta\beta$ and a_M/b_M, which are parameters to characterize a monoclinic distortion from the hexagonal symmetry, are $\Delta\beta > +0.6^\circ$ and $a_M/b_M < 1.732$ above 140 K, while $\Delta\beta < +0.6^\circ$ and $a_M/b_M \approx 1.732$ below 140 K. This suggests that the monoclinic distortion below 140 K is mainly caused by a gliding along the basal plane.

© 2009 Elsevier B.V. All rights reserved.

1. Introduction

Lithium insertion materials Li_xMeO_2, where *Me* is a transition metal element, usually vary their lattice dimensions and sometimes change their crystal symmetries with the lithium content x. The lithium cobalt dioxide Li_xCoO_2, which has been used as a positive electrode material for commercially available lithium-ion batteries, exhibits the structural variation with x at ambient temperature (T); as x decreases from 1, Li_xCoO_2 is in a rhombohedral ($R\bar{3}m$) phase with $0.75 > x > 0.56$, then a monoclinic phase ($C2/m$) with $0.56 \geq x \geq 0.51$, and finally a rhombohedral phase ($R\bar{3}m$) below 0.51 [1,2]. The structural and physical properties of Li_xCoO_2 have been studied by a microcalorimetric analysis [4], powder X-ray diffraction (XRD) [1–3], electron diffraction [5], and magnetic [6,7] measurements, especially in order to understand why the monoclinic phase appears in the narrow x range ($x \sim 0.5$).

Reimers et al. proposed that the monoclinic phase observed around $x = 0.5$ was stabilized by the ordering of Li^+ ions, and they illustrated a dome-shaped phase diagram of Li_xCoO_2 in the T range between 263 and 333 K from the characteristic signals of the $R\bar{3}m \leftrightarrow C2/m \leftrightarrow R\bar{3}m$ phases in the electrochemical data [1,3]. According to their diagram, the x range of the monoclinic phase at low T is expected to expand than that at ambient T, although there are, to our knowledge, no structural data for Li_xCoO_2 below ambient T.

In this paper, we report the result of XRD measurements on powder samples of Li_xCoO_2 with $x = 1.02$, 0.60, 0.56, and 0.53 in the T range between 90 and 300 K and discuss the structural nature of the monoclinic phase at low T.

2. Experimental

The polycrystalline sample of $LiCoO_2$ was prepared by a solid-state reaction technique using reagent grade $Li(OH)\cdot H_2O$ and $CoCO_3$ powders. The mixed powder was pressed into a pellet of 23 mm diameter and ~ 5 mm thickness. The pellet was then heated at 900 °C in air for 12 h. The crystal structure of the sample was characterized by a powder XRD (RINT-2200, Rigaku Co. Ltd., Japan) analysis. Its electrochemical property was checked by a charge and discharge test using a electrode mix of 88 wt% $LiCoO_2$, 6 wt% conducting carbon, and 6 wt% binder. The XRD analysis showed that the $LiCoO_2$ sample has a layered structure with space group of $R\bar{3}m$, in which Li^+ and Co^{3+} ions are located at 3*b* and 3*a* sites, respectively. The lattice parameters at 300 K in the hexagonal setting were estimated to be $a_H = 2.8120(1)$ Å and $c_H = 14.0303(4)$ Å. For describing the analytical errors of XRD data, we use parentheses at the last number, such as 2.8120(1) Å meaning the value of 2.8120 Å contains the error of ±0.0001 Å.

Low-T XRD measurements were performed with a synchrotron radiation using the large Debye–Scherrer camera installed at BL19B2 in SPring-8. The temperature of the sample during the XRD measurements was controlled by a cold N_2 gas flow. The wavelength of the X-ray was estimated to be 0.99772(1) Å by the XRD measurement on NIST CeO_2 standard (674a). Considering the linear

* Corresponding author. Tel.: +81 561 71 7698; fax: +81 561 63 6137.
E-mail address: e1089@mosk.tytlabs.co.jp (K. Mukai).

0378-7753/$ – see front matter © 2009 Elsevier B.V. All rights reserved.
doi:10.1016/j.jpowsour.2009.03.004

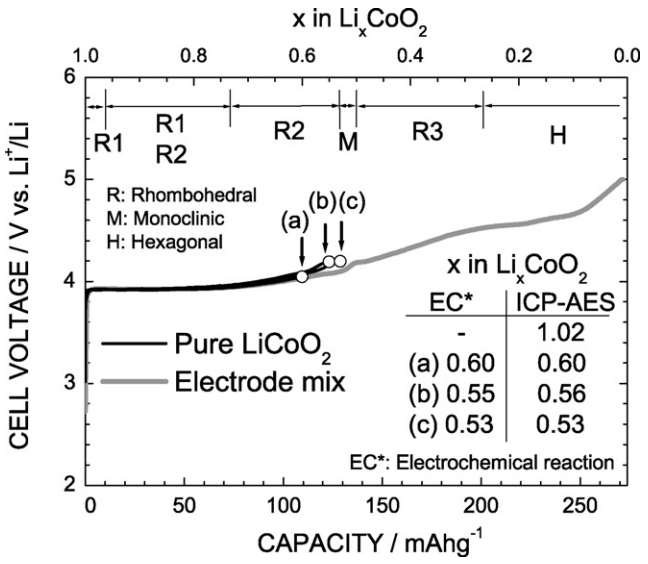

Fig. 1. The charge curves of the Li/$LiCoO_2$ cells operated at 298 K (25 °C). In order to maximize the signal-to-background ratio of the XRD pattern, the positive electrode was made of $LiCoO_2$ powder with 0.1 g for low-T XRD measurements. The Li/Co ratios were determined by an ICP–AES analysis after the XRD measurements. The charge curve of the cell using the electrode mix, consisting of 88 wt% $LiCoO_2$, 6 wt% acetylene black, and 6 wt% PVdF, is also shown. The applied current density for the pure $LiCoO_2$ and electrode mix is 0.1 and 0.28 mA cm^{-2}, respectively. R_i symbolizes the rhombohedral phase, M the monoclinic phase, and H the hexagonal phase.

attenuation coefficient of pure $LiCoO_2$ ($\sim 320\,cm^{-1}$ at 1 Å) [8], the diameter of the sample (capillary) should be minimized. In order to obtain an optimal XRD pattern, we used the pure Li_xCoO_2 sample, which was prepared by an electrochemical reaction from the pure $LiCoO_2$ electrode. The Li_xCoO_2 sample (~ 1 mg) was placed into a boro-silicate glass capillary tube with 0.3 mm diameter in an Ar-filled glove box. The chemical composition of the Li_xCoO_2 samples was determined by an inductively coupled plasma (ICP) atomic emission spectral (AES) analysis (CIROS 120, Rigaku Co. Ltd., Japan) after the XRD measurements. In this paper, we use the Li/Co ratio obtained by the ICP–AES analysis as x in Li_xCoO_2. Unit cell parameters were refined using a non-linear least squares program RIETAN-2000 [9].

3. Results and discussion

Fig. 1 shows the charge curves of the Li/$LiCoO_2$ cells operated at 298 K (25 °C). The applied current density for the electrode mix and pure $LiCoO_2$ is 0.28 and 0.1 mA cm^{-2}, respectively. As were reported previously for $LiCoO_2$ [1,2], a small change in the charge curve is clearly observed around $x = 0.5$, corresponding to the structural change among the $R\bar{3}m \leftrightarrow C2/m \leftrightarrow R\bar{3}m$ phases. This indicates that the present sample is very close to the stoichiometric $LiCoO_2$, while the ICP–AES analysis showed that Li/Co = 1.02. As seen in Fig. 1, the charge curves for the three pure $LiCoO_2$ electrodes are essentially the same to that for the electrode mix, while the curve for the pure $LiCoO_2$ electrode looks to deviate upwards at $x < 0.6$ from the curve for the electrode mix. However, the Li/Co ratio, which was determined by the ICP–AES analysis, is almost the same to the calculated value from the charge capacity (EC, see the inset in Fig. 1). This indicates that the electrochemical reaction quantitatively proceeds in the $LiCoO_2$ electrode.

Fig. 2 shows the variation of the XRD patterns with T in the 2θ range between 28.2 and 29.2° for the Li_xCoO_2 samples with $x =$ (a) 1.02, (b) 0.60, (c) 0.56, and (d) 0.53. The data were taken on cooling. Due to the structural change from the rhombohedral phase ($R\bar{3}m$) to the monoclinic phase ($C2/m$) at $x \sim 0.56$, the (1 0 4) diffraction peak splits into two peaks [(1 1 1) and (2 0 $\bar{2}$)] with the intensity ratio $I(1\,1\,1)/I(2\,0\,\bar{2}) = 2$ [1]. The $x = 1.02$ and 0.60 samples are, thus, identified to be in the rhombohedral phase, while the $x = 0.56$ and 0.53 samples are in the monoclinic phase at 300 K. For the $x = 0.56$ sample, however, an unidentified diffraction peak marked by $*$ is observed at the location between the (1 1 1) and (2 0 $\bar{2}$) peak in the T range between 140 and 300 K. The other unidentified peak also appears above the vicinity of (003) peak. In order to explain these unidentified diffraction peaks, it is most reasonable to assume the coexistence of the minor Li_xCoO_2 phase with $x \neq 0.56$ in the sample. Such peaks are also observed for the $x = 0.53$ sample at T between 190 and 300 K (see Fig. 2(d)).

For the $x = 1.02$ and 0.60 samples, as T decreases from 300 to 90 K, the (1 0 4) peak shifts toward higher diffraction angle without the split of the (1 0 4) diffraction line, indicating the absence of a structural phase transition at whole T measured. For the $x = 0.56$ and 0.53 samples, the (2 0 $\bar{2}$) and (1 1 1) peaks also shift toward a higher diffraction angle down to ~ 140 K, then both peaks broaden

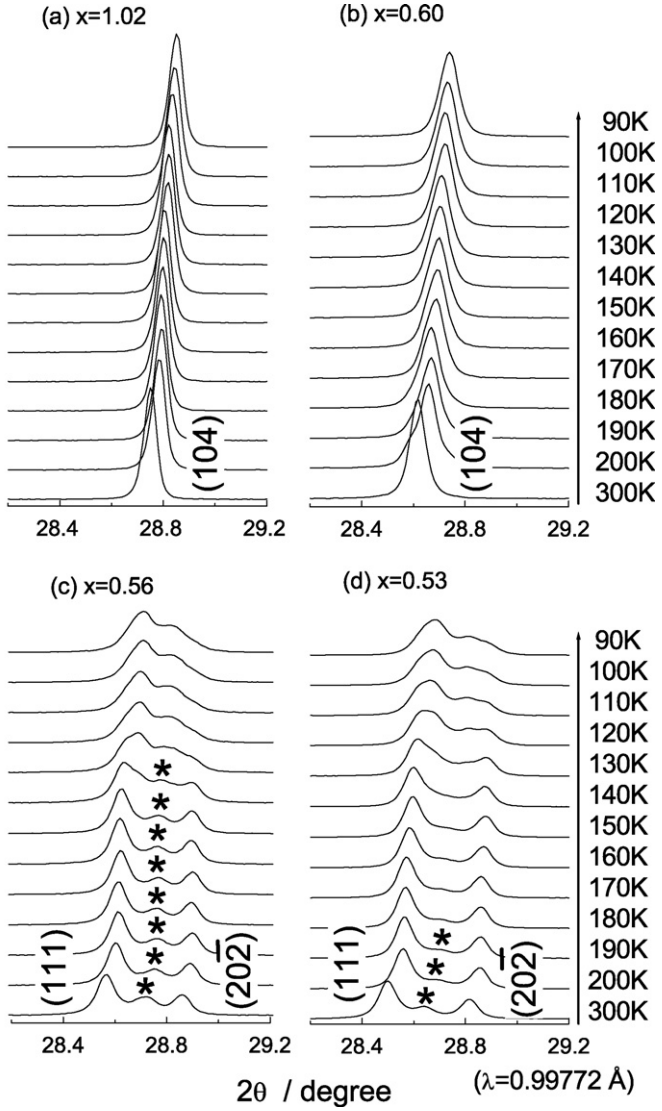

Fig. 2. XRD patterns for the Li_xCoO_2 samples with $x =$ (a) 1.02, (b) 0.60, (c) 0.56, and (d) 0.53 measured using a synchrotron radiation source in the temperatures range between 300 and 90 K. The measurements were performed on cooling. Miller indexes in (a) and (b) are given for hexagonal setting, and those in (c) and (d) for monoclinic setting. Unidentified diffraction peaks in (c) and (d) are marked by $*$.

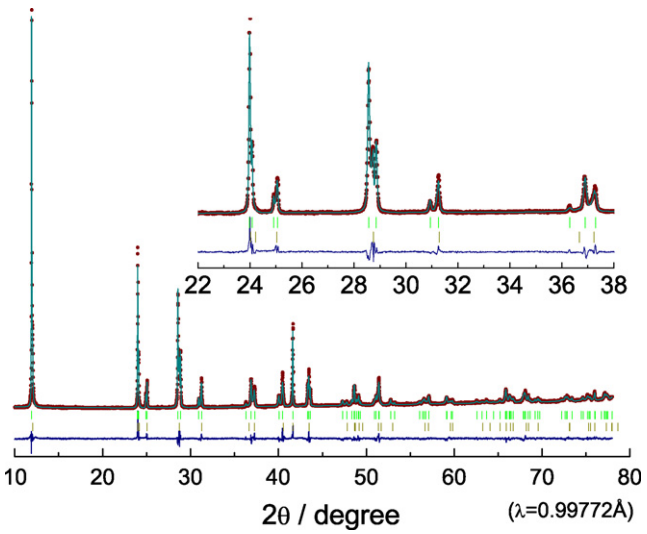

Fig. 3. Rietveld analysis for the Li_xCoO_2 sample with $x = 0.56$ at 300 K. The simulation was carried out by using a pseudo-Voigt profile function. The observed (I_{obs}) and calculated (I_{calc}) intensity data are plotted as points and solid line in the upper field. The bar-code type indications show all the possible Bragg reflections from both the major phase at the upper side and the minor at the lower side. The difference between I_{obs} and I_{calc} is shown in the lower field.

their line width. This suggests the possibility that the high-T monoclinic phase changes into the rhombohedral phase below 90 K, although the samples still have a monoclinic symmetry down to 90 K.

The T dependence of the lattice parameters was obtained by a Rietveld analysis. The effect of the minor phase on the composition of the major phase was also evaluated by the Rietveld analysis. Fig. 3 shows the analytical result for the $x = 0.56$ sample at 300 K. Assuming that the minor phase has a rhombohedral symmetry, the lattice parameters of the minor phase in the $x = 0.56$ sample are calculated to be $a_H = 2.8159(1)$ Å and $c_H = 14.3164(5)$ Å (see Table 1). Based on the x dependence of the c_H-axis at ambient T [2], the Li/Co ratio of the minor phase is determined to be 0.60(2). The weight fraction for the major and minor phase is calculated by:

$$W_p = \frac{S_p(ZMV)_p}{\sum_{i=1}^{n} S_i(ZMV)_i}, \quad (1)$$

where W is the relative weight fraction of the phase p in a mixture of the n phase, S the Rietveld scale factor, Z the number of formula units per unit cell, M the mass of the formula unit, and V the unit cell volume, respectively [9]. Because the W_{minor} is calculated to be ~ 20%, the Li/Co ratio of the major phase is determined to be 0.55(1). Similarly, the Li/Co ratio of the major phase in the $x = 0.53$ sample is estimated to be 0.52(1) and that for the minor phase 0.58(2) ($W_{minor} \sim 18\%$). The Li/Co ratio of the major phase is, therefore, comparable to that of the ICP–AES analysis and eventually the effect of the minor phase on the composition of the major phase is negligibly small.

Although the $x = 1.02$ and 0.60 samples are in a rhombohedral symmetry in the whole T range measured, their lattice parameters are converted into those in the monoclinic setting, in order to compare the lattice parameters for the four samples as a function of T. Fig. 4(a) shows the structural relationship between the hexagonal and monoclinic setting. The hexagonal lattice parameters are transformed into those in the monoclinic setting using the following equations:

$$\begin{aligned} a_M &= \sqrt{3} \times a_H, \\ b_M &= a_H, \\ c_M &= \frac{c_H}{3 \sin \beta_M}, \quad \text{and} \\ \beta_M &= 180^\circ - \tan^{-1} \frac{c_H}{\sqrt{3} a_H}, \end{aligned} \quad (2)$$

where M denotes the monoclinic setting and H the hexagonal setting. Fig. 5 shows the T dependence of (a) a_M-, (b) b_M-, and (c) c_M-axes for the Li_xCoO_2 samples with $x = 1.02$, 0.60, 0.56, and 0.53. The c_M-axis length decreases monotonically with decreasing T, while the T dependence of the a_M- and b_M-axis is very small. More correctly, for the $x < 1.02$ samples, its thermal expansion coefficient is estimated to be $3.0 - 4.2 \times 10^{-5}$ K^{-1} along the c_M-axis, and

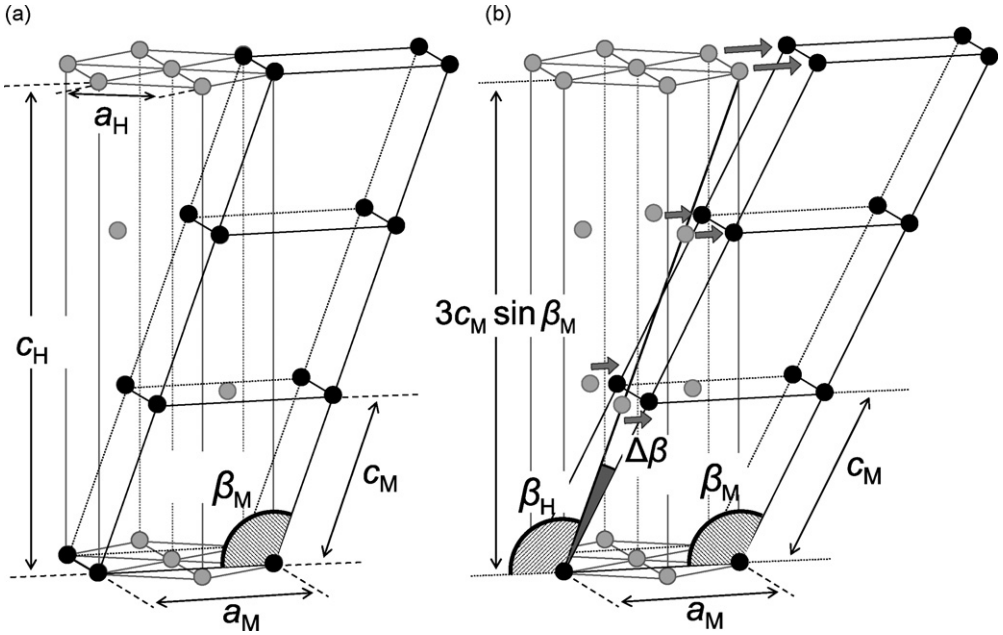

Fig. 4. The structural relationship between hexagonal and monoclinic setting. The crystal structure is in the (a) hexagonal and (b) monoclinic phase. β_M and β_H are the angle between a_M- and c_M-axis, and an ideal hexagonal angle in the monoclinic phase, respectively. The value of $\Delta\beta$ ($= \beta_H - \beta_M$) in (b) indicates the degree of distortion from the hexagonal phase along the c_H-axis.

Table 1
The structural parameters determined by the Rietveld analysis for the $x = 0.56$ sample at 300 K.

Phase	Space group	Atom	Wyckoff position	g	x	y	z	Lattice parameter	B_{iso}[a] (Å^2)
Major phase	$C2/m$	Li1	2*d*	0.55	0	1/2	1/2	$a_M = 4.8760(2)$ Å	3.98(5)
		Co1	2*a*	1.0	0	0	0	$b_M = 2.8168(1)$ Å	1.05(1)
		O1	4*i*	1.0	0.735(1)	0	0.200(1)	$c_M = 5.0640(2)$ Å	1.69(2)
								$\beta_M = 107.929(2)^\circ$	
Minor phase	$R\bar{3}m$	Li2	3*b*	0.60	0	0	1/2	$a_H = 2.8159(1)$ Å	3.98(5)
		Co2	3*a*	1.0	0	0	0	$c_H = 14.3164(5)$ Å	1.05(1)
		O2	6 *c*	1.0	0	0	0.262(1)		1.69(2)

The reliability factor and goodness-of-fit indicator are $R_{wp} = 2.84\%$ and $s = 1.26$, respectively. The weight fraction of the minor phase (W_{minor}) is calculated to be ~ 20%.
[a] Constrains : B (Li1) = B (Li2), B (Co1) = B (Co2), B (O1) = B (O2).

$0.2 - 1.0 \times 10^{-5}\,K^{-1}$ along the a_M-axis. This means that the interplane distance between the adjacent CoO_2 planes is very sensitive to T, such as ~ 10 times larger than that for the distance between the nearest neighboring Co ions in the CoO_2 plane. This is consistent with the fact that the CoO_2 plane is formed by a rigid network of edge-sharing CoO_6 octahedra.

Fig. 6(a) shows the T dependence of β_M for the Li_xCoO_2 samples with $x = 1.02$, 0.60, 0.56, and 0.53. For the $x = 1.02$ and 0.60 samples, β_M increases slightly with decreasing T, due to the anisotropic lattice shrinkage. For the $x = 0.56$ and 0.53 samples, as T decreases from 300 K, β_M increases monotonically down to 150 K, then rapidly increases with changing the slope ($d\beta_M/dT$) between 140 and 120 K, and finally seems to level off to a constant value below 100 K.

There are two parameters to characterize a monoclinic distortion from the hexagonal symmetry; namely, $\Delta\beta$ defined by Eq. (3)(see Fig. 4(b)) and a_M/b_M.

$$\Delta\beta = \beta_H - \beta_M = \left(180^\circ - \tan^{-1}\left(\frac{3c_M \sin\beta_M}{a_M}\right)\right) - \beta_M, \qquad (3)$$

where $\Delta\beta$ correlates with the distortion along the interplane and a_M/b_M corresponds to the distortion in the plane. As seen in Fig. 6(b), $\Delta\beta$ is ~ +0.7° for the $x = 0.56$ sample and $\Delta\beta$ is ~ +0.8° for the $x = 0.53$ sample at 300 K. Although $\Delta\beta$ decreases with decreasing T, $\Delta\beta$ ranges between + 0.3 and +0.4° even at 90 K for the two samples. The values of a_M/b_M for the $x = 0.56$ and 0.53 samples are ~ 1.731 in the T range between 140 and 300 K, and then reach ~ $\sqrt{3}$ below 120 K, where $a_M/b_M = \sqrt{3}$ is the value for the hexagonal symmetry (see Fig. 6(c)). The transition T between the high-T and low-T monoclinic phases is found to be 140 K. The monoclinic phase above 140 K is characterized by $\Delta\beta > +0.6^\circ$ and $a_M/b_M < 1.732$, while that below 140 K is characterized by $\Delta\beta < +0.6^\circ$ and $a_M/b_M \approx 1.732$. Note that both $\Delta\beta = 0$ and $a_M/b_M = \sqrt{3}$

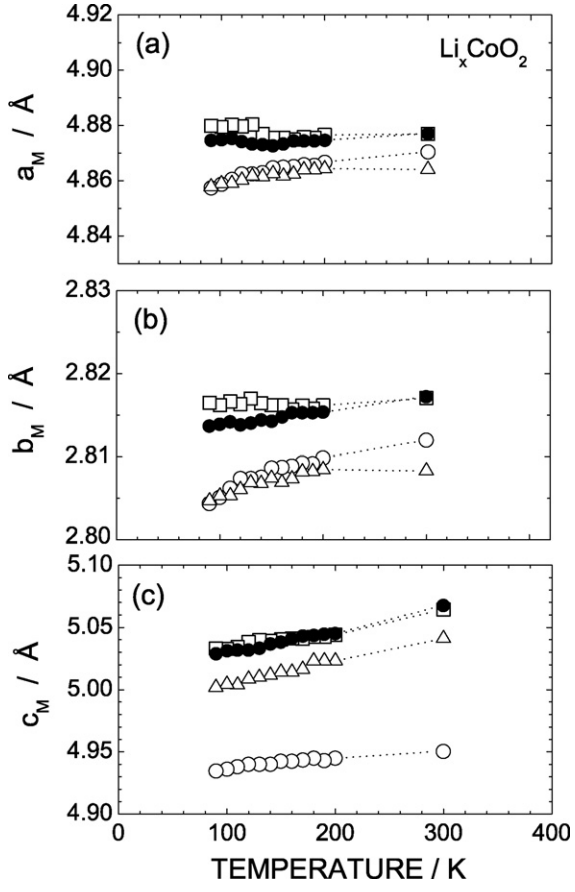

Fig. 5. Temperature dependence of the lattice parameters of (a) a_M-, (b) b_M-, and (c) c_M-axes for the Li_xCoO_2 samples with $x = 1.02$ (○), 0.60 (△), 0.56 (□), and 0.53 (•). All the lattice parameters are converted into the values in monoclinic setting using Eq. (2).

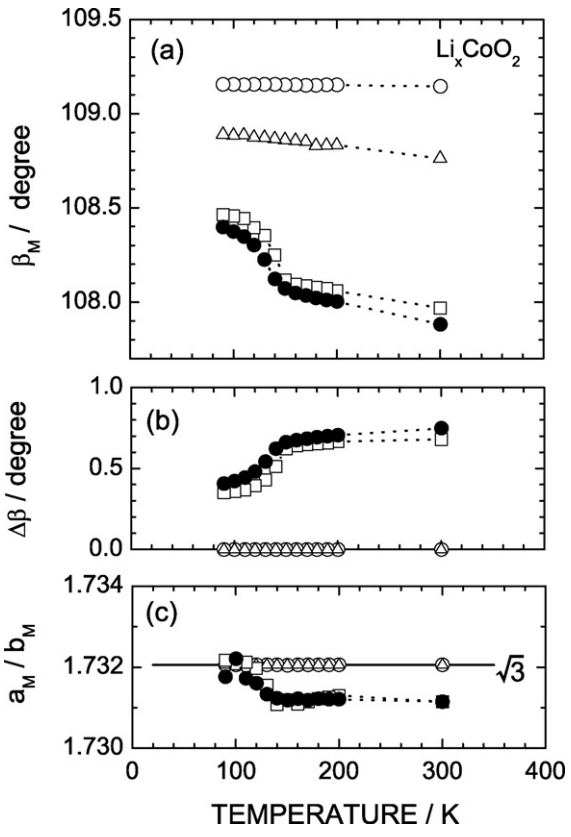

Fig. 6. Temperature dependences of (a) β_M, (b) $\Delta\beta$, and (c) a_M/b_M ratio for the Li_xCoO_2 samples with $x = 1.02$ (○), 0.60 (△), 0.56 (□), and 0.53 (•). $\Delta\beta$ is calculated using Eq. (3). The solid line in (c) represents the a_M/b_M value (= $\sqrt{3}$) for a hexagonal symmetry.

should be satisfied for a hexagonal phase. The low-T monoclinic phase around 100 K shows that $a_M/b_M = 1.732$, which is equivalent to that for the hexagonal lattice. Since $\Delta\beta$ is larger by $+0.4^\circ$ than that for hexagonal lattice, the monoclinic distortion below 120 K is mainly caused by a gliding along the basal plane. In other words, only the CoO_6 stacking sequence along c_H-axis slightly deviates from that required for the hexagonal setting. It should be noted here that the monoclinic phase observed for Li_xCoO_2 with $x \sim 0.5$ is different from that observed for Li_xNiO_2 [10]. This is because $\Delta\beta$ for Li_xNiO_2 with $0.75 \geq x \geq 0.45$ is $\sim -0.2^\circ$ at ambient T, and a_M/b_M is ~ 1.76.

In summary, we have examined the low-T crystal structure for the monoclinic phase with $x = 0.56$ and 0.53 in Li_xCoO_2. Although the origin of such a monoclinic phase, that we observed in the limited x range, is still unknown, the character of the monoclinic phase at ambient T is distinguishable from the monoclinic phase at low T in terms of the degree of monoclinic distortion from the hexagonal lattice, $\Delta\beta$ and a_M/b_M. The T dependences of $\Delta\beta$ and a_M/b_M suggest that the x range for the monoclinic phase at low T is likely to be narrower than that at ambient T ($0.56 \geq x \geq 0.51$). However, the XRD data below 90 K is currently unavailable, because of the limitation on the cooling system of liquid nitrogen. The low-T examinations together with the macro- and microscopic magnetic measurements will give more insight into the possible origin of monoclinic distortion from the hexagonal lattice for the layered lithium insertion materials.

Acknowledgements

This experiment was performed at the SPring-8 with the approval of the Japan Synchrotron Radiation Research Institute (Proposal No. 2007A1917). We thank the staff of SPring-8 for help with the XRD measurements. We also appreciate Dr. I. Tajima of TCRDL for XRD measurements at SPring-8 and Mr. Y. Kondo of TCRDL for ICP–AES analysis. This work is partially supported by Grant-in-Aid for Scientific Research (B), 1934107, MEXT, Japan.

References

[1] J.N. Reimers, J.R. Dahn, J. Electrochem. Soc. 139 (1992) 2091–2097.
[2] T. Ohzuku, A. Ueda, J. Electrochem. Soc. 141 (1994) 2972–2977.
[3] J.N. Reimers, J.R. Dahn, U. von Sacken, J. Electrochem. Soc. 140 (1993) 2752–2754.
[4] J.J. Auborn, Y.L. Barberio, J. Electrochem. Soc. 134 (1987) 638–641.
[5] Y. Shao-Horn, S. Levasseur, F. Weill, C. Delmas, J. Electrochem. Soc. 150 (2003) A366–A373.
[6] S. Kikkawa, S. Miyazaki, M. Koizumi, J. Solid State Chem. 62 (1986) 35–39.
[7] K. Mukai, Y. Ikedo, H. Nozaki, J. Sugiyama, K. Nishiyama, D. Andreica, A. Amato, P.L. Russo, E.J. Ansaldo, J.H. Brewer, K.H. Chow, K. Ariyoshi, T. Ohzuku, Phys. Rev. Lett. 99 (2007) 087601.
[8] A.J.C. Wilson, E. Prince (Eds.), International Tables for Crystallography, vol. C, 2nd ed., Kluwer Academic, Dordrecht, 1999.
[9] F. Izumi, T. Ikeda, Mater. Sci. Forum 198 (2000) 321–324.
[10] T. Ohzuku, A. Ueda, M. Nagayama, J. Electrochem. Soc. 140 (1993) 1862–1870.